International Journal of Nanomedicine

Dovepress
open access to scientific and medical research

Open Access Full Text Article

ORIGINAL RESEARCH

Development of resveratrol-conjugated gold nanoparticles: interrelationship of increased resveratrol corona on anti-tumor efficacy against breast, pancreatic and prostate cancers

This article was published in the following Dove Press journal:
International Journal of Nanomedicine

Velaphi C Thipe[1,2]
Kiandohkt Panjtan Amiri[3]
Pierce Bloebaum[2,4]
Alice Raphael Karikachery[2,5]
Menka Khoobchandani[2,5]
Kavita K Katti[2,5]
Silvia S Jurisson[1,6]
Kattesh V Katti[2,4–7]

[1]Department of Chemistry, University of Missouri, Columbia, MO 65201, USA; [2]Institute of Green Nanotechnology, University of Missouri, Columbia, MO 65211, USA; [3]Department of Physics, Washington University, St. Louis, MO 63130, USA; [4]Department of Physics and Astronomy, [5]Department of Radiology, [6]University of Missouri Research Reactor, University of Missouri, Columbia, MO 65211, USA; [7]Department of Medical Pharmacology and Physiology, University of Missouri, Columbia, MO 65211, USA

Background: As part of our continuing quest to enhance the efficacy of bioactive phytochemicals in cancer therapy, we report an innovative green nanotechnology approach toward the use of resveratrol for the production of biocompatible resveratrol-conjugated gold nanoparticles (Res-AuNPs). Our overarching aim is to exploit the inherent pro-apoptotic properties of gold nanoparticles (AuNPs) through synergistic anti-tumor characteristics of resveratrol, with the aim of developing a new class of green nanotechnology-based phytochemical-embedded AuNPs for applications in oncology.

Method: Resveratrol was used to reduce Au^{3+} to Au^{0} for the synthesis of Res-AuNPs at room temperature and gum arabic (GA) was used to further encapsulate the nanoparticulate surface to increase the overall stability of the AuNPs. This comprehensive study involves the synthesis, full characterization and in vitro stability of Res-AuNPs in various biological media for their ultimate applications as anti-cancer agents against human breast (MDAMB-231), pancreatic (PANC-1) and prostate (PC-3) cancers.

Results: This strategy to systematically increase the corona of resveratrol on AuNPs, in order to gain insights into the interrelationship of the phytochemical corona on the overall anti-tumor activities of Res-AuNPs, proved successful. The increased resveratrol corona on Res-AuNPs showed superior anti-cancer effects, attributed to an optimal cellular uptake after 24-hour incubation, while GA provided a protein matrix support for enhanced trans-resveratrol loading onto the surface of the AuNPs.

Conclusion: The approach described in this study harnesses the benefits of nutraceuticals and nanoparticles toward the development of Res-AuNPs. We provide compelling evidence that the increased corona of resveratrol on AuNPs enhances the bioavailability of resveratrol so that therapeutically active species can be optimally available in vivo for applications in cancer therapy.

Keywords: resveratrol, gold nanoparticles, nanotechnology, cancer therapy

Introduction

Cancer is one of the largest causes of death worldwide. In 2015, one in six deaths globally were due to cancer, and cancer metastasis is the major cause of increased death, accounting for 8.8 million deaths.[1] Approximately 1,735,350 new cancer cases were projected, predominantly including 268,670, 55,440 and 164,690 cases of breast, pancreatic and prostate cancer, respectively.[2–4] Breast and prostate cancer are the most commonly diagnosed cancers in women and men, respectively, and

Correspondence: Kattesh V Katti
One Hospital Drive, Columbia, MO 65212, USA
Tel +1 573 882 5656
Fax +1 573 884 5679
Email KattiK@health.missouri.edu

submit your manuscript | www.dovepress.com
DovePress
http://doi.org/10.2147/IJN.S204443

pancreatic cancer is the fourth leading cause of cancer death and one of the most aggressive cancers to treat.[5–8] Although clinical management of these cancers has increased considerably over the past decade, current modalities still suffer from lack of effectiveness of the therapy owing to drug permeability inside the tumor as a result of the highly abnormal blood vessels (<200 nm diameter). Surgery, chemotherapy and radiotherapy are common treatments used for these cancers, although surgery often leads to tumor recurrence and other complications that result in postoperative complications.[4,9–12] Chemotherapy and radiotherapy suffer from non-selective uptake and delivery of drugs and/or high-energy deposition (gamma rays, X-rays or ion beams) because of their inability to differentiate between normal healthy cells and cancerous cells, thereby causing severe systemic toxic effects in patients.[4,12]

Researchers have explored a number of avenues to overcome these challenges, with limited success. The application of a phytochemical-derived plant-based holistic approach for cancer therapy is gaining considerable prominence throughout the world, as the World Health Organization in its latest forecast stated that over 80% of the global population will use some form of holistic medicine in health and hygiene.[13,14] It has been long known that phytochemicals present highly beneficial effects on the human body through their dual role as disease-preventive and curative agents for the prevention and treatment of various chronic diseases.[15] Various phytochemicals exhibit high antioxidant activity that, in turn, is responsible for modulating multiple cell signaling pathways (eg, nuclear factor-κB), thus exerting their preventive and therapeutic effects.[16,17] Resveratrol (trans-3,5,4′-trihydroxystilbene), a phenolic compound predominantly present in the skin of red grapes and in red wine, as shown in Figure 1,[18] is one of many phytochemicals, and has been highly investigated for its efficacy in disease prevention and treatment, including in cancer.

Resveratrol has been reported to possess anti-angiogenic, anti-inflammatory, anti-proliferative, anti-cancer and antioxidant properties.[19] However, like many other plant-based phytochemicals in medicine, resveratrol suffers from poor bioavailability once administered in vivo owing to its susceptibility to rapid enzymatic degradation by the body's innate immune system well before it can exert its therapeutic influence, formation of conjugates with glucuronic acid, and sulfate accumulation in plasma and urine.[19–21] This translates to inadequate resveratrol concentrations circulating in the body and reaching the tumor;[4] therefore, a drug design that allows for high delivery of resveratrol to cancerous cells will be beneficial. Resveratrol has two isomers, trans-resveratrol and cis-resveratrol, as shown in Figure 2; resveratrol

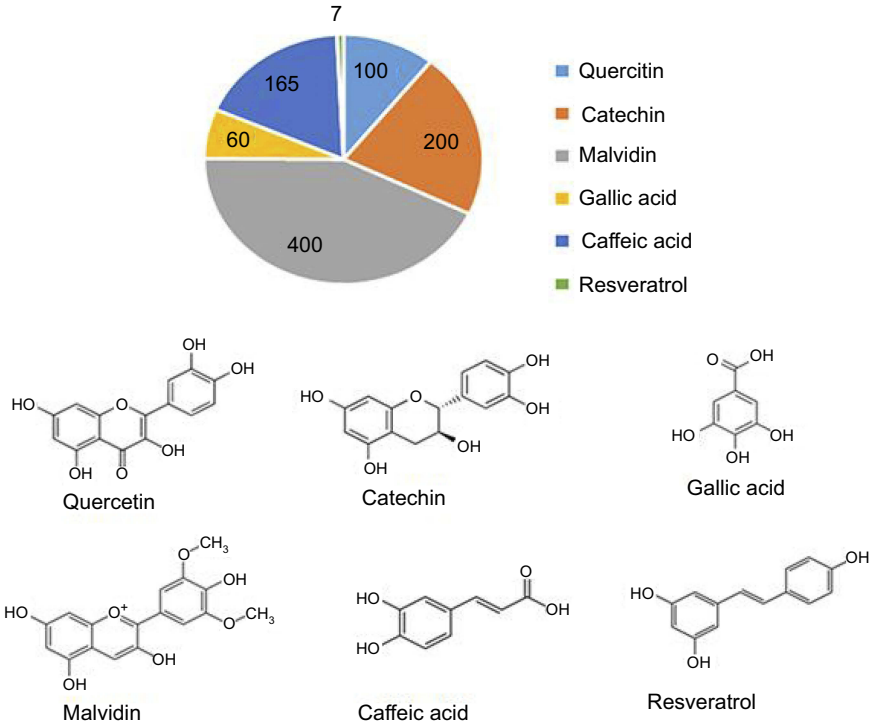

Figure 1 The amount of major polyphenols in red wine (mg/mL) and their chemical structures.
Note: Data from Xiang et al.[18]

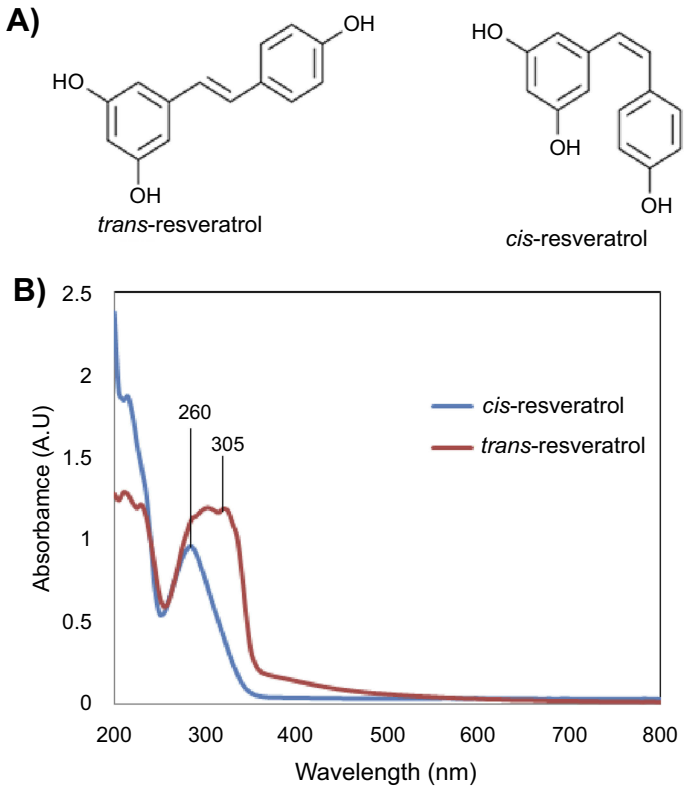

Figure 2 Isomers of resveratrol: (**A**) structural and (**B**) ultraviolet–visible spectrum differences.

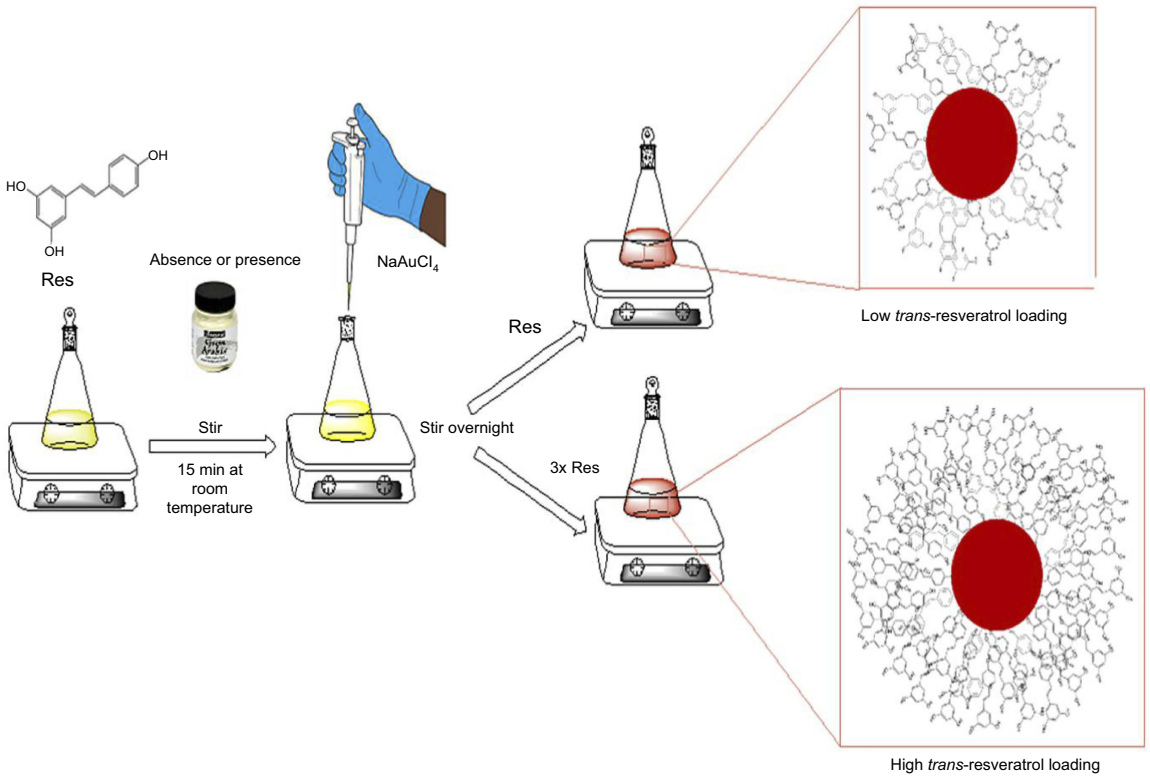

Scheme 1 Synthetic route for resveratrol gold nanoparticles (Res-AuNPs) and resveratrol-gum arabic- conjugated gold nanoparticles (Res-GA-AuNPs). The 3x Res to increase the resveratrol corona around the AuNPs.

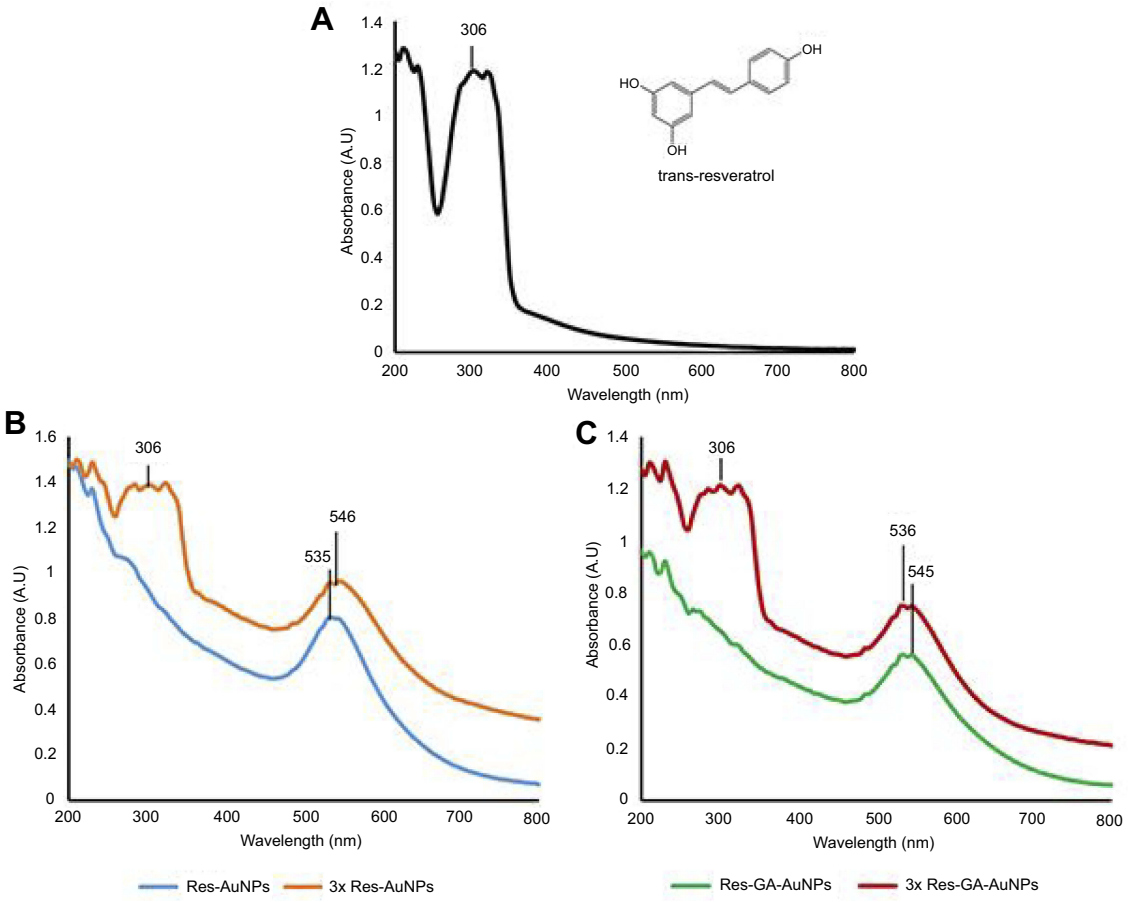

Figure 3 Ultraviolet–visible spectrum: (**A**) trans-resveratrol used in the reaction; (**B**) AuNPs in the absence of GA; and (**C**) AuNPs in the presence of GA. The threefold increase in resveratrol significantly increased the AuNP-conjugated trans-resveratrol molecules.
Abbreviations: Res, resveratrol; AuNPs, gold nanoparticles; GA, gum arabic.

predominantly exists in the trans configuration.[22] The cis isomer has been reported to lack any pharmacological activity owing to rapid glucuronidation, which results in a lower bioavailability and effectiveness.[23] Allan et al[24] reported the absorptivity of the trans-resveratrol solution, absorbing at 305 nm (4.07 eV), and cis-resveratrol at 260 nm (4.77 eV).

For phytochemical-based medicines to become more effective in treating cancers and various other debilitating diseases, it is imperative to develop innovative strategies to enhance the biological half-lives of therapeutic phytochemicals.[4,12] As part of our pioneering strategy to apply green nanotechnology in the design of nanoceuticals,[12,16,17,25–44] we herein report an innovative green nanotechnology approach towards the use of resveratrol as a reducing and stabilizing agent for the synthesis of biocompatible resveratrol-conjugated gold nanoparticles (Res-AuNPs).[45] We report the comprehensive characterization of Res-AuNPs using ultraviolet–visible (UV-vis) spectrophotometry, dynamic light scattering (DLS), quantitative liquid chromatography-mass spectrometry–multiple reaction monitoring (LC-MS-MRM) and transmission electron microscopy (TEM). We also report the in vitro stability of Res-AuNPs in various biological media for their ultimate applications as a new generation of green nanotechnology-based anti-cancer agents against human breast (MDAMB-231), pancreatic (PANC-1) and prostate (PC-3) cancers.

This paper reports on our successful strategy to systematically increase the corona of resveratrol on AuNPs, as part of our efforts to gain insights into the interrelationship of the phytochemical corona with the overall anti-tumor activities of Res-AuNPs. A threefold increase in the resveratrol corona on Res-conjugated AuNPs showed superior anti-cancer effects owing to the high resveratrol corona around the AuNPs' surface. Dark-field microscopic (CytoViva) images revealed that 3× Res-AuNPs had an optimal cellular uptake after 24-hour incubation. A synergistic approach facilitated by gum arabic (GA) increased the overall stability and provided a protein matrix support for enhanced trans-resveratrol loading onto the surface of the AuNPs.

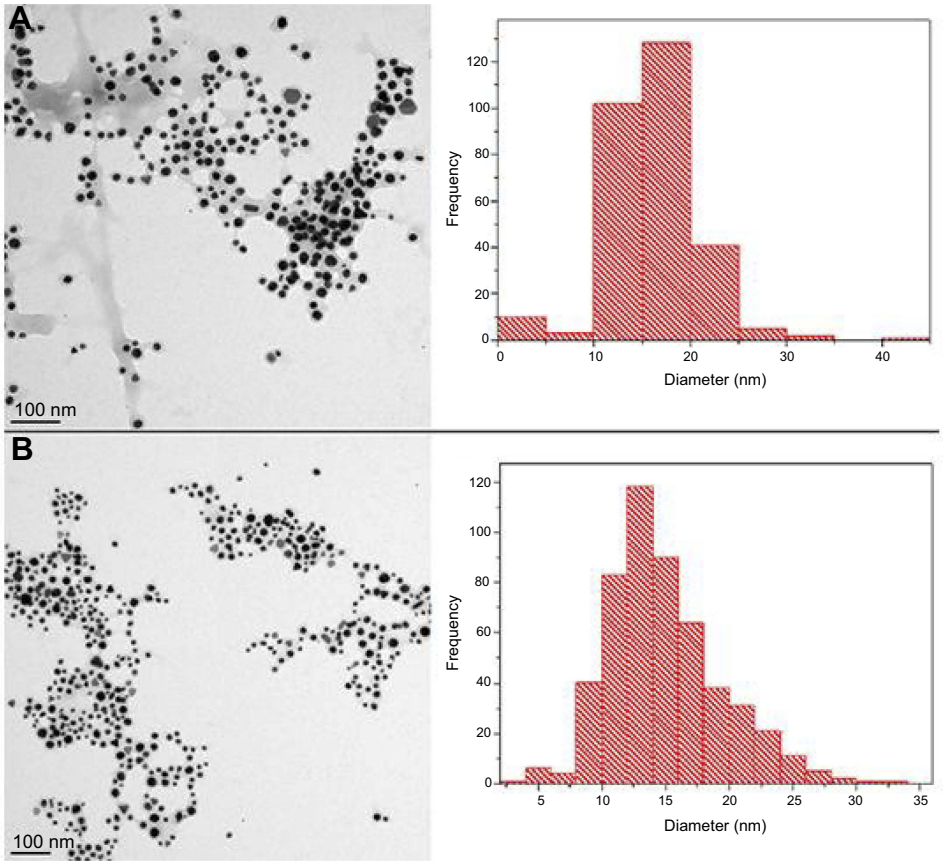

Figure 4 Transmission electron microscope images of AuNPs and size distribution: (**A**) Res-AuNPs; (**B**) Res-GA-AuNPs.
Abbreviations: AuNPs, gold nanoparticles; Res, resveratrol; GA, gum arabic.

Materials and methods

Materials

Resveratrol ≥99% (HPLC), 99% sodium tetrachloroaurate (III) dihydrate ($NaAuCl_4$), DL-cysteine 97%, BSA and human serum albumin (HSA) lyophilized powder, sodium chloride (NaCl), PBS, DAPI, MTT and trypan blue were all purchased from Sigma-Aldrich Chemical Company (St Louis, MO, USA). L-Histidine 98%, GA and TrypLE Express were from Thermofisher Scientific (Waltham, MA, USA), while FBS, DMEM media and RPMI media were obtained from Life Invitrogen (New York, NY, USA). Breast (MDAMB-231), pancreatic (PANC-1) and prostate (PC-3) cancer cells were obtained from the American Type Culture Collection (ATCC, Manassas, VA, USA).

Characterization of Res-AuNPs and Res-GA-AuNPs

The surface plasmon resonance (SPR) of AuNPs and the absorption measurements of the conjugated Res- and Res-GA molecules were recorded using Varian Cary 50 UV-vis spectrophotometers (Agilent Technologies, Santa Clara, CA, USA). The hydrodynamic size and the surface charge were determined using a Zetasizer Nano ZS (Malvern Instruments, Northampton, MA, USA) and the core size was measured using the JEOL-1400 transmission electron microscope (TEM) (JEOL, Tokyo, Japan) while the high resolution TEM images were collected on the FEI Tecnai F30 G2 Twin TEM. The size distribution was determined with ImageJ 1.50i software by processing the TEM images. Surface conjugation and functional groups were determined by Fourier-transform infrared spectroscopy (FTIR) using the Thermo Nicolet Nexus 4700 FT-IR Spectrometer (Thermofisher Scientific, Waltham, MA, USA). The amount of conjugated Res molecules was determined by liquid chromatography–mass spectrometry–multiple reaction monitoring (LC-MS-MRM) (Thermofisher Scientific, USA). The in vitro cellular viability measurements were determined using the SpectraMax M2 microplate reader (Molecular Devices, LLC, San Jose, CA, USA).

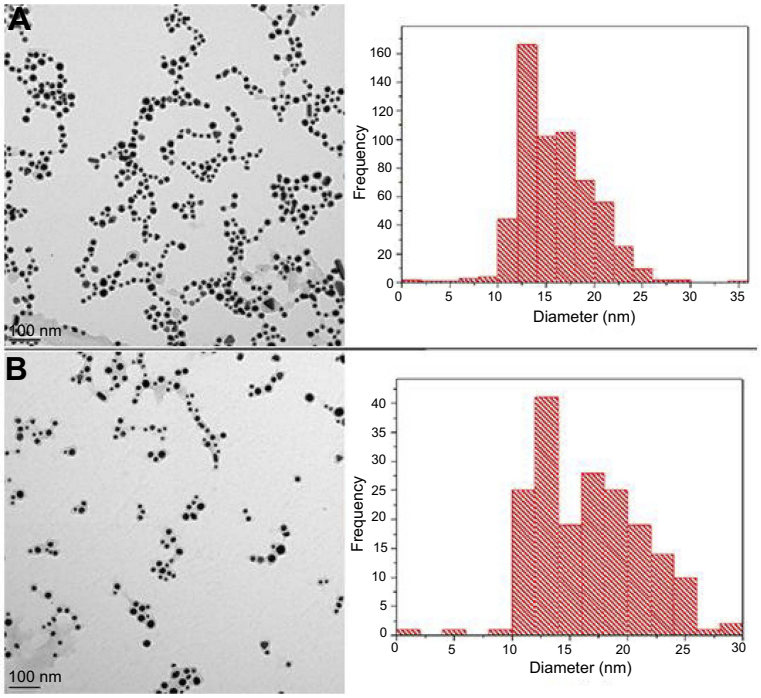

Figure 5 Transmission electron microscope images of AuNPs and size distribution: (**A**) 3× Res-AuNPs; (**B**) 3× Res-GA-AuNPs.
Abbreviations: AuNPs, gold nanoparticles; Res, resveratrol; GA, gum arabic.

Table 1 Physicochemical data parameters of Res-AuNPs and Res-GA-AuNPs

Sample	Res-AuNPs	3× Res-AuNPs	Res-GA-AuNPs	3× Res-GA-AuNPs
Size (nm)				
Hydrodynamic size	56.1	107.7	64.1	187.7
Core size	16.1±5.0	16.0±4.0	14.9±4.4	16.7±4.6
Capping	40	91.8	49.2	171
Zeta potential (mV)	−25	−26	−22	−24
Au concentration (μg/mL)[a]	142	150	153	162
Resveratrol				
Res concentration (μg/mL)[b]	187	423	188	408
AuNPs per mL	7.3×10^{12}	7.6×10^{12}	9.4×10^{12}	6.7×10^{12}

Notes: [a]Inductively coupled plasma atomic emission spectroscopy; [b]Folin–Ciocalteu polyphenol concentration.
Abbreviations: Res, resveratrol; AuNP, gold nanoparticle; GA, gum arabic.

Resveratrol-conjugated gold nanoparticles (Res-AuNPs)

The Res-AuNPs were synthesized using the following approaches to investigate the amount of trans-resveratrol molecules conjugated onto the surface of the AuNPs.

Resveratrol gold nanoparticles (Res-AuNPs)

The synthesis of Res-AuNPs was carried out in the absence of GA. In brief, resveratrol (2 mg) was added to 6 mL of deionized water and the reaction mixture was stirred at room temperature for 10 minutes. To the reaction mixture, 100 μL of 0.1 M $NaAuCl_4$ (in deinoized water) was added while stirring and the mixture was allowed to stir overnight to achieve optimal resveratrol capping. The formation of AuNPs was evident based on the mixture's color change from yellow to a clear dark red solution, which was characterized by UV-vis absorption spectroscopy, Zetasizer Nano and TEM instrumentation techniques.

Utility of gum arabic to stabilize resveratrol-encapsulated gold nanoparticles (Res-GA-AuNPs)

We have applied our pioneering research on the utility of US Food and Drug Administration (FDA)-approved GA protein to stabilize AuNPs.[29,32,35,36,40,42] The synthesis of Res-GA-AuNPs was carried out in the presence of GA. In brief, resveratrol (2 mg) and GA (3 mg) were added to 6 mL doubly deionized water. The mixture was stirred for 10 minutes and 100 μL of 0.1 M $NaAuCl_4$ (in deionized water) was added while stirring at room temperature. The mixture was kept on a magnetic stirrer overnight and then characterized by UV-vis absorption spectroscopy, Zetasizer and TEM instrumentation techniques.

Resveratrol corona effect on gold nanoparticles (3× Res-AuNPs and 3× Res-GA-AuNPs)

The amount of resveratrol used in the reaction mixture was increased to 6 mg based on the above-mentioned methods

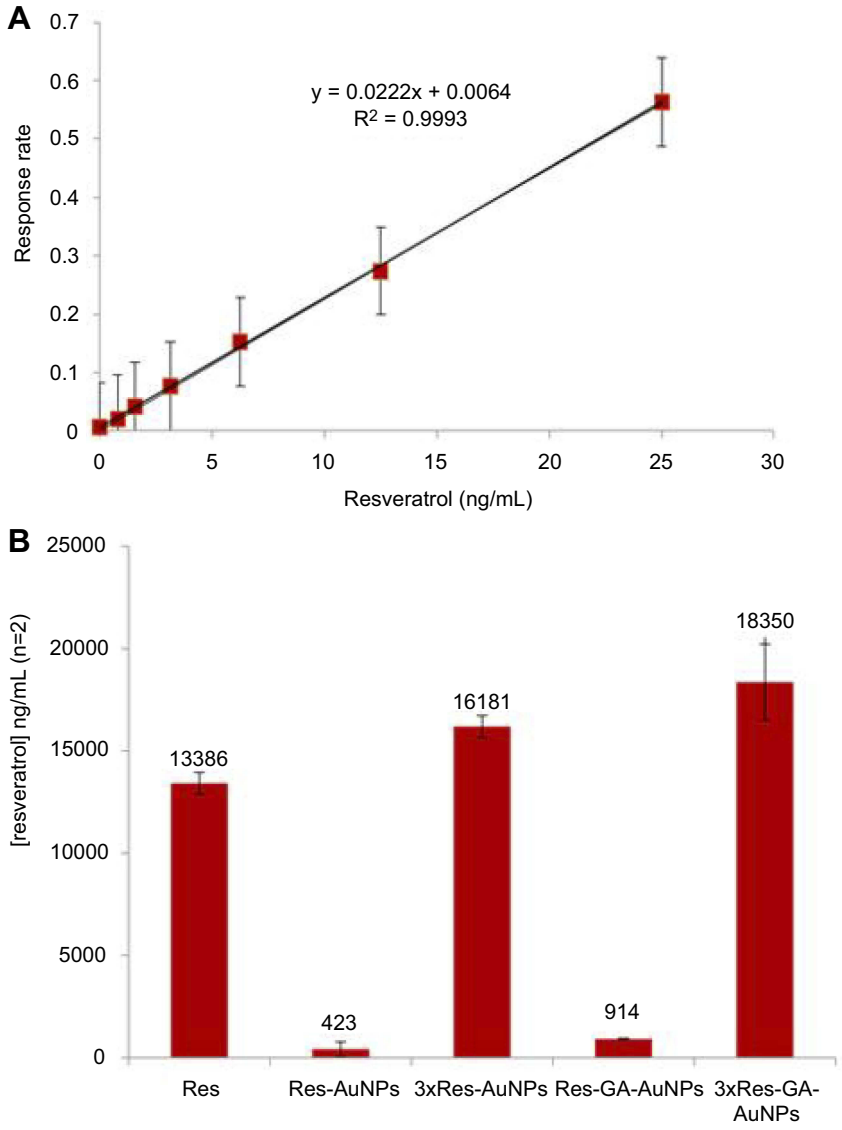

Figure 6 Liquid chromatography–multiple reaction monitoring of (**A**) Res standard curve and (**B**) Res-conjugated AuNPs. The signal (AUC) for resveratrol was normalized to the AUC for tolbutamide internal standard. The average response (AUC-mangiferin/AUC-tolbutamide; AUC-RES/AUC-Tol) from triplicate injections was plotted. Linearity for resveratrol was good (R^2>0.99) across the entire calibration range.
Abbreviations: Res, resveratrol; AuNPs, gold nanoparticles; GA, gum arabic; AUC, area under the curve.

for the synthesis of 3× Res-AuNPs and 3× Res-GA-AuNPs to increase the number of trans-resveratrol-conjugated molecules on the surface of AuNPs.

In vitro stability study of Res-, 3× Res-, Res-GA- and 3× Res-GA-AuNPs

The in vitro stability of the AuNPs was investigated in the presence of different biological fluids (ie, 0.5% BSA, 0.5% HSA, 0.5% cysteine, 0.2 M histidine, 1% NaCl, RPMI and DMEM media, PBS at pH 5, pH 7 and pH 9). In brief, 200 µL of AuNPs was added to 1.5 mL microcentrifuge tubes, each containing 800 µL of each biological solution, and incubated for 1 hour, 24 hours and 1 week at room temperature. The stability was measured by recording the SPR peak of the AuNPs using UV-vis spectrophotometry.

Quantification of resveratrol molecules on the surface of AuNPs

Folin–Ciocalteu phenol quantification

A standard curve was generated using known concentrations of resveratrol (500, 250, 125, 62.5, 31.3 and 15.6 µg/mL). Using the standard curve, the amount of resveratrol was determined by extrapolation. In brief, 1 mL of Res-AuNPs was added to a 5 mL centrifuge tube and 500 µL of 1:10 Folin–Ciocalteu phenol reagent and 1 mL of 7.5% (w/v) sodium carbonate solution were added to the tube. The tube

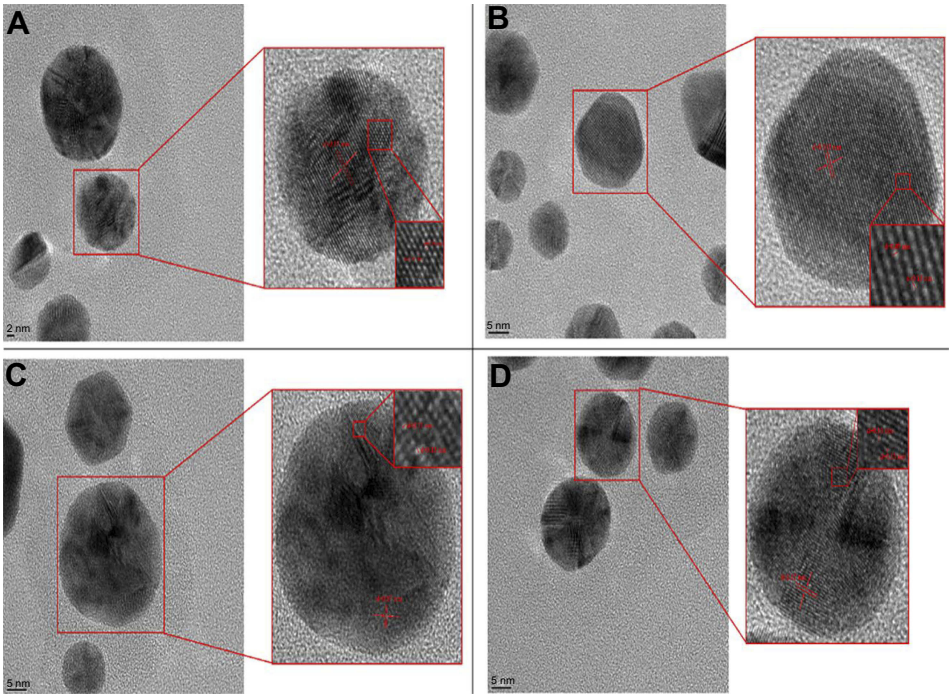

Figure 7 High-resolution transmission electron microscopy images of AuNPs demonstrating lattice fringes: (**A**) Res-AuNPs: *d*=0.17 nm, (**B**) 3× Res-AuNPs: *d*=0.14 nm, (**C**) Res-GA-AuNPs: *d*=0.17 nm, and (**D**) 3× Res-GA-AuNPs: *d*=0.17 nm.
Abbreviations: AuNPs, gold nanoparticles; Res, resveratrol; GA, gum arabic.

was incubated at 30°C for 30 minutes in the dark, and a SpectraMax M2 microplate reader was used to determine the amount of resveratrol by measuring at 750 nm.

LC-MS-MRM

The amount of resveratrol conjugated to the surface of the AuNPs was further quantified using LC-MS-MRM on a Quantiva instrument (Thermofisher, USA). Method development was conducted to determine MRM transitions for resveratrol and its retention time on the column. The AuNPs were centrifuged at 16,000 × *g* in a microcentrifuge tube and the supernatant was diluted 1:10,000 with an internal standard solution (30 ng/mL tolbutamide in 5% acetonitrile/1% formic acid). Then 25 µL aliquots were transferred into autosampler vials and placed in a cooled (7°C) autosampler. An MRM transition consists of a precursor–fragment pair that allows the mass spectrometer (Thermo Scientific TSQ Quantiva QQQ) to ignore every molecule in a sample except the resveratrol to facilitate accurate quantitation with very high specificity and sensitivity. To specifically quantify the resveratrol, two optimized transitions were generated, as follows. The stock solution of Res (2.5 mg/mL in ethanol) was diluted 1:1,000 in 70% acetonitrile/0.1% formic acid. This solution was then analyzed by direct infusion (3 µL/min). Prominent peaks for the +1 ion of resveratrol (228.25 g/mol) were observed and fragmentation was optimized. The tolbutamide (internal standard) was optimized with the following ionization conditions: ionization voltage 1,600 V, Q1 and Q3 resolution 0.7 (full-width half-maximum), collision gas 1.5 mTorr, collision energy at 32 eV, dwell time 200 ms and source temperature 120°C. Quantification was performed using MRM with transitions of m/z 271→91 for tolbutamide (internal standard). Thereafter, 30 ng/mL internal standard solvent and 25 ng/mL resveratrol were injected onto the C_{18} column, and retention times were determined.

In vitro cell viability efficacy of AuNPs

The AuNPs were investigated for their in vitro anti-cancer cell viability efficacy against breast (MDAMB-231), pancreatic (PANC-1) and prostate (PC-3) cancer cell lines using the MTT cell proliferation assay, performed according to the manufacturer's recommendations. In brief, 100 µL of 4×10^4 cells of each cell line in the exponential growth phase were seeded in each well of a flat-bottomed 96-well polystyrene-coated plate and the plates were incubated at 37°C for 24 hours in a CO_2 incubator at 5% CO_2 atmosphere. The cells were incubated with different concentrations of AuNPs (200–6.3 µg/mL) and free resveratrol at different concentrations (200–6.3 µg/mL) for 24 and 48 hours. After incubation, 10 µL of MTT dye (stock solution 5 mg/mL in PBS) was added and the plates were incubated for 3 hours. After

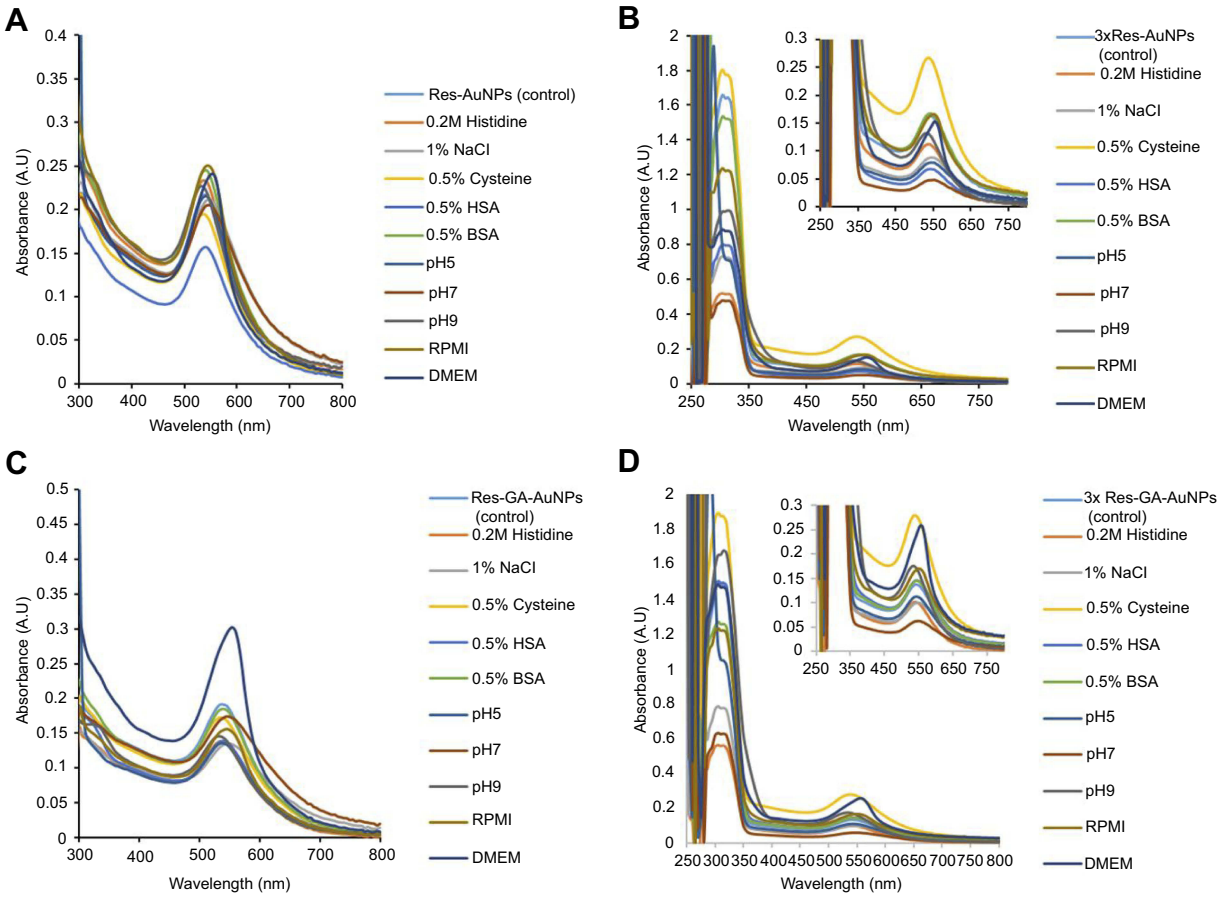

Figure 8 In vitro stability study of (**A**) Res-AuNPs, (**B**) 3× Res-AuNPs (insert, magnified plasmon peak), (**C**) Res-GA-AuNPs, and (**D**) 3×Res-GA-AuNPs (insert, magnified plasmon peak) in different biological media after 24 hours.
Abbreviations: Res, resveratrol; AuNPs, gold nanoparticles; GA, gum arabic.

Table 2 Anti-tumor IC_{50} (μg/mL) cell viability efficacy of AuNPs

Sample	Cancer cells		
	MDAMB-231	PANC-1	PC-3
Res-AuNPs	N/A	N/A	N/A
3× Res-AuNPs	40	79	38
Res-GA-AuNPs	N/A	200.4	N/A
3× Res-GA-AuNPs	72	72	59

Abbreviations: AuNP, gold nanoparticle; Res, Resveratrol; GA, gum arabic; MDAMB-231, breast cancer; PANC-1, pancreatic cancer; PC-3, prostate cancer; N/A, not applicable.

3-hour incubation, the formed formazan crystals were dissolved in 100 μL of DMSO and the intensity of the developed color was measured by a SpectraMax M2 microplate reader (Molecular Devices, LLC, San Jose, CA, USA) operated at 570 nm wavelength. All experiments were performed three times in quadruplicate, and the percentage of cell viability was calculated using the formula: $[(T/C) \times 100]$, where C = absorbance of control and T = absorbance of treatment. The half-maximal inhibitory concentration (IC_{50}) was determined using GraphPad Prism Version 6.01 software.

Cellular uptake of Res- and Res-GA-AuNPs

Cellular internalization of AuNPs using dark-field CytoViva microscopy

In vitro cellular internalization (endocytosis) analysis of AuNPs was performed using a dark-field CytoViva microscopic technique. Ultraclean and sterile coverslips were kept in six-well plates and 8×10^5 cells per well were seeded into six-well plates in media (DMEM for MDAMB-231 and PANC-1 cells, and RPMI for PC-3 cells) and incubated for 24 hours in a 5% CO_2 incubator at 37°C. Res-AuNPs, 3× Res-AuNPs, Res-GA-AuNPs and 3× Res-GA-AuNPs (50 μg/mL) were added to cells, followed by 2-, 4- and 24-hour incubation at 37°C. After incubation, the cells were washed with 1× PBS (1 mL) and fixed with 1 mL 4% paraformaldehyde in PBS that had been incubated in the dark at room temperature for 15 minutes. Thereafter, the cells were further washed three times with cold 1× PBS (1 mL). Slides were prepared using DAPI nuclear dye and the slides were observed under CytoViva dark-field microscopy coupled with dual-mode fluorescence. Cell morphology was initially

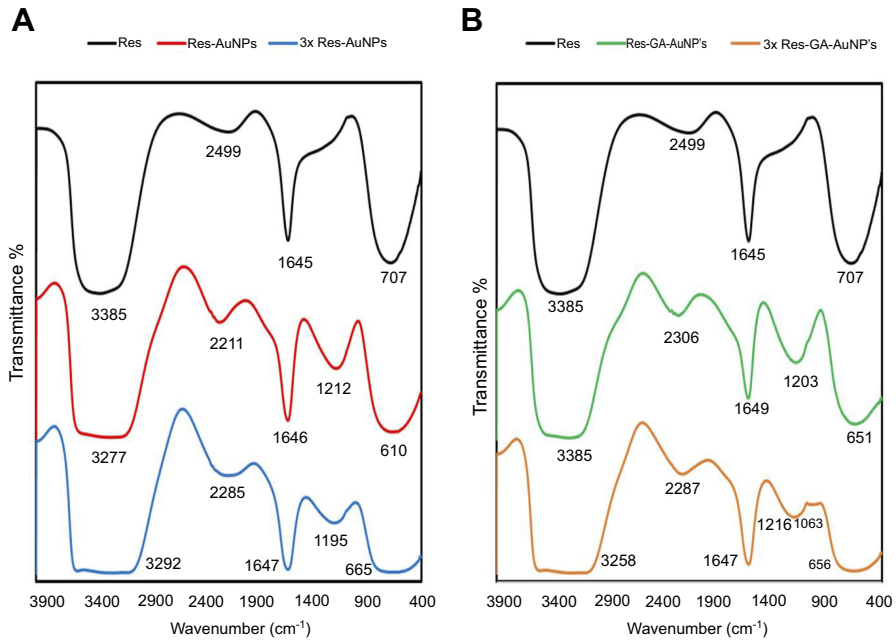

Figure 9 Infrared spectrum of: (**A**) Res-AuNPs; 3× Re-AuNPs and (**B**) Res-GA-AuNPs; 3× Res-GA-AuNPs.
Abbreviations: Res, resveratrol; AuNPs, gold nanoparticles; GA, gum arabic.

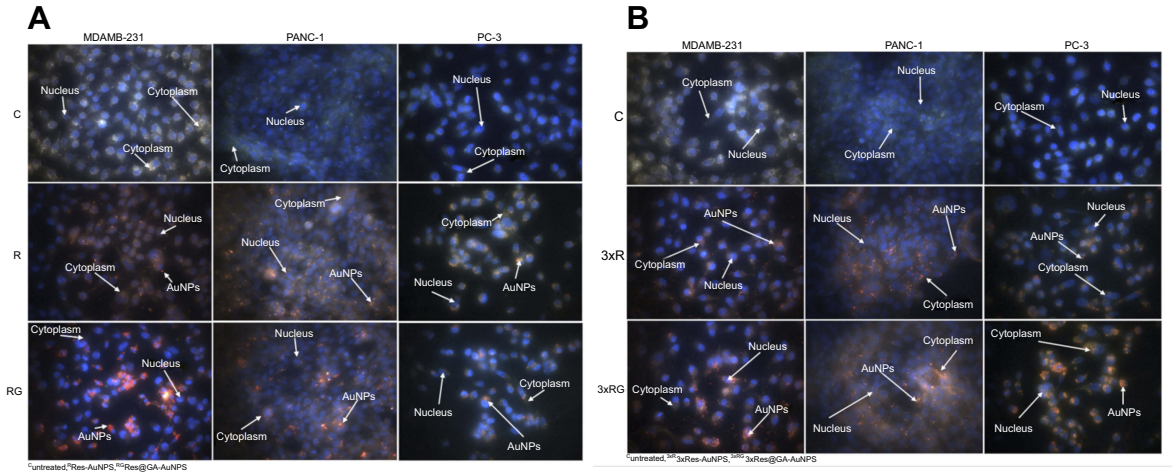

Figure 10 (**A**) Cellular internalization of Res-AuNPs and Res-GA-AuNPs in breast (MDAMB-231), pancreatic (PANC-1) and prostate (PC-3) cancer cell lines incubated for 24 hours at 42 µg/mL. (**B**) Cellular internalization of 3× Res-AuNPs and 3× Res-GA-AuNPs in MDAMB-231, pancreatic and prostate cancer cell lines incubated for 24 hours at 42 µg/mL.
Abbreviations: Res, resveratrol; AuNPs, gold nanoparticles; GA, gum arabic.

observed, followed by uptake of AuNPs. Images were captured via Dage Imaging Software at 40× magnification.

Statistical analysis

Statistical analysis was performed using GraphPad Prism Version 6.01 software (GraphPad Software, San Diego, CA, USA). Statistical evaluation was measured using the two-way ANOVA test to verify the effects of treatment. The IC_{50} was determined to compare the average of the treatment group to the average of the control group. Statistical tests with $p<0.05$ were considered significant. All results are presented as mean ± SEM.

Results and discussion

Synthesis and characterization of Res-AuNPs and Res-GA-AuNPs

In our green nanotechnology investigations, as discussed in the following sections, we have focused on the

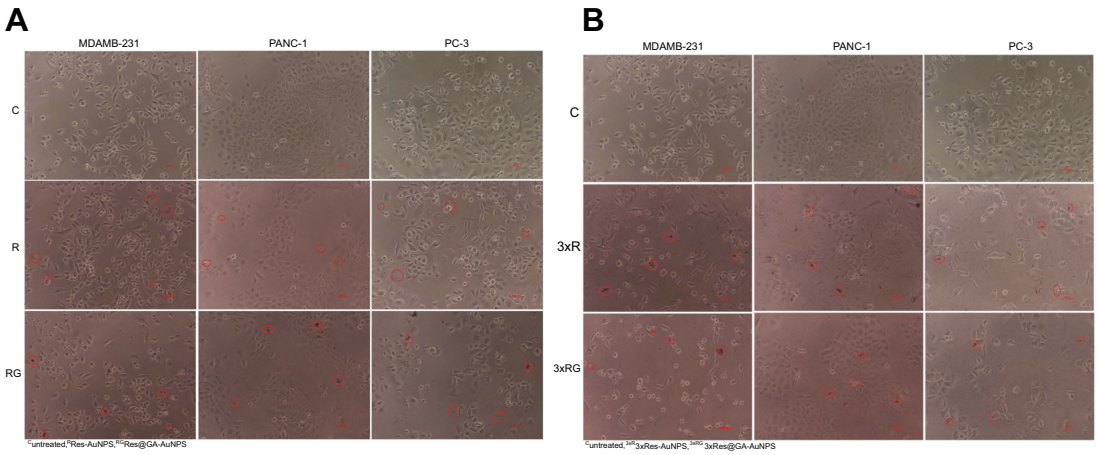

Figure 11 (**A**) Cellular morphological changes after treatment with Res-AuNPs and Res-GA-AuNPs for 24 hours. (**B**) Cellular morphological changes after treatment with 3× Res-AuNPs and 3× Res-GA-AuNPs for 24 hours. The red circles show the cell debris, representing cell death.
Abbreviations: Res, resveratrol; AuNPs, gold nanoparticles; GA, gum arabic.

production of resveratrol-conjugated AuNPs with varying corona of the phytochemical for subsequent investigations of their anti-tumor efficacy. We have also focused on the role of GA as an encapsulating agent on AuNPs in order to explore the applicability of this plant-based protein to enhance the corona of resveratrol bound to AuNPs.[12]

GA is a natural complex polysaccharide composed of highly branched units in glycoproteins and polysaccharides.[46,47] Species of *Acacia senegal* and *Acacia seyal*, which are indigenous to the African continent, have a high content of GA, which is used as a stabilizer in the food industry.[48] Because of its highly branched structure, GA can improve the stability of nanoparticles by providing a support matrix for drug loading and delivery.[40,42,48] Extensive research on AuNPs as a delivery carrier has shown effective delivery of biomolecules and drugs.[4] This is attributed to the high surface area-to-volume ratio of AuNPs, which allows for increased phytochemical conjugation. AuNPs also offer the advantage of being a contrast agent for in vivo imaging and for therapeutic applications.[4,12,35,49,50]

Recent studies have demonstrated that AuNPs significantly improved the diagnostic and therapeutic capabilities of nanomedical products. For example, AuNPs are used in biosensor development for signal amplification owing to their optical and electrochemical sensing capabilities.[51] Moreover, AuNPs have demonstrated promise in the advancement of cancer treatment by inhibiting cell proliferation, activating a cascade of pathways to induce apoptosis,[25,26,31,35,38,40,42,52] affecting mitochondrial functioning and inhibiting cell migration.[53–60] Despite considerable past efforts in the diagnosis and therapy of cancer, there is still a continuing pursuit toward discovering effective modalities that limit the side effects caused by current treatments. We postulated that GA would provide a supportive matrix for increased trans-resveratrol conjugation onto AuNPs, thus allowing subsequent delivery of the therapeutic phytochemical for cancer treatment. To validate this hypothesis, we have embarked on: 1) the green synthesis of Res-GA-AuNPs and 2) complete characterization of AuNPs for stability and cellular internalization. Overall, this work is focused on increasing the trans-resveratrol corona conjugated on AuNPs and a GA matrix to increase resveratrol bioavailability for synergistic therapeutic effects of both resveratrol and biocompatible AuNPs. The results reported herein also considered that the development of effective nano-nutraceutical modalities for cancer therapy is of paramount importance in achieving high therapeutic benefits for patients, because surgery, chemotherapy and radiation present high risks affecting a patient's quality of life.

Resveratrol was used because of its potency as a natural anticancer agent.[19,61–65] The molecular electron density and chemical reactivity of the cis- and trans-resveratrol isomers mean that they play a fundamental role as antioxidants as well as chelating agents for metal ions. The redox properties of resveratrol provide a surface potential via the hydroxyl groups. Quantum chemical calculations have revealed that resveratrol has a high electronegativity (χ) value at 3.23 eV, thus facilitating the reduction of Au^{3+} to Au^{0} through its phenolic O–H bond dissociation enthalpy, and a large χ value demonstrates a potent anti-inflammatory activity.[66] In the present study, we have investigated the optimal incorporation and stabilization of Res-AuNPs and Res-GA-AuNPs by increasing the trans-resveratrol-conjugated molecules on the surface of AuNPs. The stability of Res-AuNPs, synthesized in the presence of GA, was

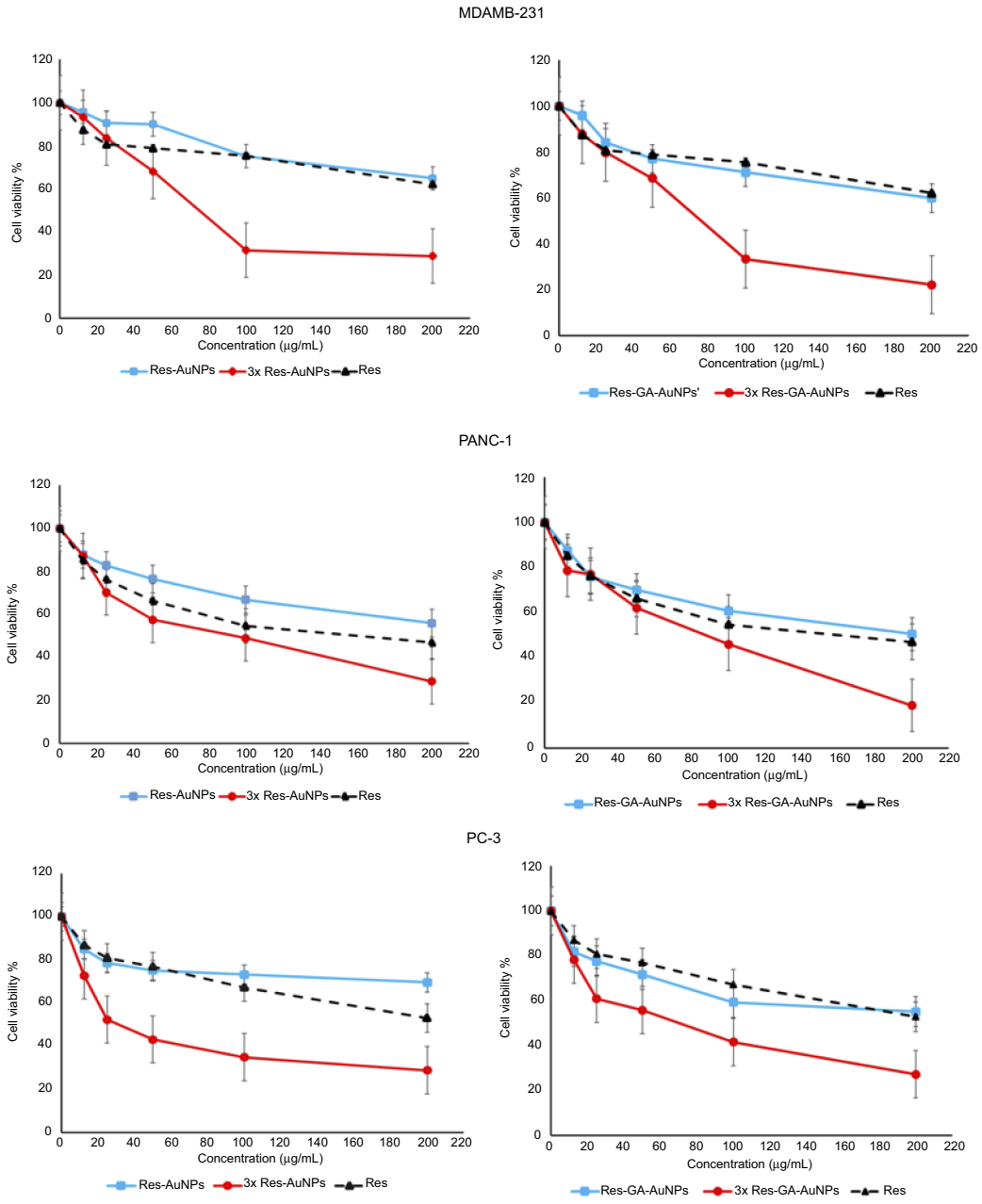

Figure 12 Effectiveness of Res-AuNPs and Res-GA-AuNPs on cell viability of breast (MDAMB-231), pancreatic (PANC-1) and prostate (PC-3) cancer cells.
Abbreviations: Res, resveratrol; AuNPs, gold nanoparticles; GA, gum arabic.

evaluated in biological media in comparison with Res-AuNPs without GA. The concentration of resveratrol was increased to form multiple layers of resveratrol corona on the surface of AuNPs to achieve optimum corona effects, as shown in Scheme 1.

The efficacy of AuNPs as anti-tumor agents was evaluated against breast, pancreatic and prostate cancer cells (MDAMB-231, PANC-1 and PC-3, respectively). The Res-AuNPs were produced by reacting specific amounts of resveratrol molecules (333 µg/mL) with $NaAuCl_4$ in the absence and presence of GA. The successful production of AuNPs was corroborated by spectrophotometric measurements, evident in the SPR peak at 535 and 545 nm for Res-AuNPs and Res-GA-AuNPs, respectively. Similar SPR peaks were reported by Khoobchandani et al,[44] Gamal-Eldeen et al,[42] Geraldes et al,[41] Pasanphan et al[67] and Suganthy et al.[45] Moreover, the UV-vis spectra for the three-fold samples (3× Res-AuNPs and 3× Res-GA-AuNPs) show a 306 nm peak indicating increased trans-resveratrol coating onto the surface of AuNPs (Figure 3).

Further characterization of Res-AuNPs using the Zetasizer Nano ZS provided the hydrodynamic size and the surface charge of Res-AuNPs with and without GA. The TEM images revealed that the core sizes of the Res-AuNPs and Res-GA-AuNPs were 16.1±5.0 and 14.9±4.4 nm, respectively, as shown in Figure 4. The 3× Res-AuNPs and 3× Res-GA-AuNPs, as expected, showed an increase in the hydrodynamic size, indicative of the increased trans-resveratrol molecule conjugation onto the surface of the AuNPs. The results obtained from TEM images indicate that the 3× Res-AuNPs and 3× Res-GA-AuNPs have core sizes of 16.0±4.0 and 16.7±4.6 nm, respectively (Figure 5). The TEM images confirmed that the AuNPs are sufficiently mono-dispersed and spherical. There was no significant change in core size between the 1× Res- and 3× Res-AuNPs in the absence or presence of GA. The negative surface charge revealed that Res-AuNPs show no tendency to agglomerate, thus confirming their stability. The overall physicochemical parameters are summarized in Table 1.

The amount of resveratrol molecules conjugated to the surface of AuNPs was quantified using LC-MS-MRM on the Quantiva, as shown in Figure 6. The Res-AuNPs (423 ng/mL) and Res-GA-AuNPs (914 ng/mL) have significantly lower amounts of resveratrol loading compared to 3× Res-AuNPs in the overall transformation where Res reduces the Au^{3+} to Au^{0} and subsequently surface coats the AuNPs. On the other hand, 3× Res-AuNPs (16,181 ng/mL) and 3× Res-GA-AuNPs (18,350 ng/mL) have 38-fold and 20-fold increases in the amount of resveratrol molecules on the AuNPs, respectively.

The high-resolution TEM images revealed that Res AuNPs are highly crystalline. The lattice fringes *d*-spacing values between the lattice planes are 0.17, 0.14, 0.17 and 0.17 nm for Res-AuNPs, 3× Res-AuNPs, Res-GA-AuNPs and 3× Res-GA-AuNPs, respectively (Figure 7).[45] The sizes of individual Au^{0} atoms are: Res-AuNPs: d=0.135 nm; 3× Res-AuNPs: d=0.11 nm; Res-GA-AuNPs: d=0.12 nm; and 3× Res-GA-AuNPs: d=0.13 nm, where d is the space between two planes of gold atoms in a crystal.

In vitro stability studies

In vitro stability of Res-AuNPs and Res-GA-AuNPs was evaluated by monitoring the surface plasmon resonance peak (λ_{max}) over a 24-hour incubation in biological media (0.2 M histidine, 0.5% cysteine, 1% NaCl solution, 0.5% HSA, 0.5% BSA, PBS at pH 5, pH 7 and pH 9) as shown in Figure 8. The plasmon peak of Res-AuNPs and Res-GA-AuNPs demonstrated excellent stability after 24 hours; this was due to the electrostatic repulsion of the high surface negative zeta potential showing no tendency of the AuNPs to aggregate. Moreover, it is of paramount importance for in vivo therapy applications that the trans-resveratrol conjugated onto the AuNPs remains intact for an optimum length of time to provide anti-cancer effects in vivo. Our data unequivocally demonstrate that trans-resveratrol molecules on the surface of AuNPs are stable, thus showing potential for delivering optimal therapeutic efficacy in cancer therapy (see Tables 1 and 2).

FTIR spectroscopy was used to investigate the functional group conjugation of resveratrol on the surface of AuNPs. The spectral data of Res-AuNPs, 3× Res-AuNPs, Res-GA-AuNPs and 3× Res-GA-AuNPs revealed the presence of hydroxyl groups due to the broad absorption centered between 3,277 and 3,385 cm^{-1} from the conjugated resveratrol and GA molecules, respectively. The peaks between 2,211 and 2,306 cm^{-1} correspond to aliphatic C–H bonds and the bands between 1,646 and 1,649 cm^{-1} are due to the carboxylate C–O bond.[45] The peaks between 1,212 and 1,203 cm^{-1} are attributed to the phenol C–O stretching, which suggests that the resveratrol molecules are conjugated to the AuNPs via this bond, as shown in Figure 9. Moreover, the 3× Res-GA-AuNP spectral data showed a very weak peak at 1,063 cm^{-1} due to C–N stretching shift. The peaks in the 610–670 cm^{-1} range represent the O–H out-of-plane bend. This FTIR spectrum confirmed the conjugation of resveratrol molecules on the surface of AuNPs, and is corroborated by similar data reported by Suganthy et al.[45]

Cellular internalization study by dark-field microscopy

The cellular internalization of Res-AuNPs and Res-GA-AuNPs was evaluated by CytoViva dark-field optical microscopy after 2-, 4- and 24-hour incubation periods in MDAMB-231, PANC-1 and PC-3 cancer cells. Dark-field microscopic images suggested that Res-AuNPs and Res-GA-AuNPs are efficiently internalized into tumor cells within 2 hours of treatment, with optimum cellular uptake occurring between 4 and 24 hours of treatment, as shown in Figure 10A and B. The nucleus of the cell is stained by DAPI (blue color), the cytoplasm appears as a white color around the nucleus and nanoparticles are depicted by bright orange spots. An increase in incubation time is directly proportional to increased cellular internalization; this was further confirmed by the localization of the AuNPs within the cells. The results revealed a significant uptake of AuNPs into cancer cells at 24-hour incubation, suggesting that resveratrol biomolecules conjugated to AuNPs enhance phytochemical drug carrier capabilities for direct cancer therapy applications.

Cellular morphological study of Res-AuNPs and Res-GA-AuNPs

The cellular morphological integrity of the cells treated with Res-AuNPs and Res-GA-AuNPs was investigated by confocal microscopy 24 hours post-incubation. Our results indicate that the cellular density, post-incubation with Res-AuNPs, decreased, while cellular debris representing cell death was prevalent in all treated cells, as shown in Figure 11A. The results for the threefold AuNP showed highly pronounced effectiveness in cell death (Figure 11B), thus validating our hypothesis on the interrelationship between the amount of resveratrol loading on AuNPs and effective cancer therapy. Our cellular images strongly indicate evidence of apoptotic events, which include nuclear condensation, cell shrinkage, fragmentation and dysfunction, suggesting a point-of-no-return apoptotic cancer cell destruction.

Cell viability study of Res-AuNPs and Res-GA-AuNPs against MDAMB-231, PANC-1 and PC-3 cells

We have performed a comprehensive investigation on the cellular viability effectiveness of Res-AuNPs, Res-GA-AuNPs (including their threefold counterparts), free resveratrol and free GA against MDAMB-231, PANC-1 and PC-3 cancer cells. The results provide compelling evidence that the anti-tumor efficacy was concentration dependent. The threefold resveratrol corona on AuNPs (3× Res-AuNPs and 3× Res-GA-AuNPs) showed significantly more effective anti-cancer characteristics compared to 1× Res-AuNPs and Res-GA-AuNPs (Figure 12 and Table 2). The effectiveness of free resveratrol molecules was similar to that of 1× Res-AuNPs and Res-GA-AuNPs. Overall, the 3× Res-AuNPs and 3× Res-GA-AuNPs showed the highest efficacy, and this is attributed to the increased *trans*-resveratrol cargo onto the AuNPs.

Conclusions

The MTT assay results clearly show that the higher corona of Res onto AuNPs maintains tight binding of the phytochemical onto the plethora of gold atoms on the AuNP surface. This interaction, with or without the GA, provides excellent loading of the phytochemical with consequent efficient anti-tumor effects, as shown for breast, prostate and pancreatic tumor cells (Figures 11 and 12). The hydrodynamic sizes with enhanced corona of resveratrol (3× Res-AuNPs) are still within the range (<200 nm diameter) allowing efficient penetration/endocytosis of AuNPs across tumor cells.[68–70] The entry of Res-AuNPs into tumor cells provides synergistic anti-tumor effects owing to the natural anti-angiogenesis properties of AuNPs. Production of a range of combinations of AuNPs using the anti-tumor Res phytochemical, along with AuNPs, therefore provides dual anti-tumor effects, from both the AuNPs and the phytochemical, for applications of this class of nanomaterials in tumor therapy. Combinations of resveratrol and other phytochemicals with gold metal, referred to as Swarna Bhasma, have been extensively used in the Indian Ayurvedic medicine for thousands of years in treating various diseases and disorders. The resveratrol-functionalized gold nanoparticles, as described in this paper, may be considered as a modern equivalent of the Ayurvedic Medicine 'Swarna Bhasma' for potential applications in the Holistic approach to medicine.

Abbreviation list

FTIR, Fourier-transform infrared spectroscopy; GA, gum arabic; HSA, human serum albumin; LC-MS-MRM, liquid chromatography–mass spectrometry–multiple reaction monitoring; MDAMB-231, braest cancer cell line; PANC-1, pancreatic cancer cell line; PC-3, prostate cancer cell line; Res, resveratrol; SPR, surface plasmon resonance; TEM, transmission electron microscopy; UV-vis, ultraviolet–visible.

Acknowledgments

The authors thank the University of Missouri Institute of Green Nanotechnology, the South African National Research Foundation (grant number 98141) and the Fulbright Program (grant number 15150089) for providing financial support.

Disclosure

The authors report no conflicts of interest in this work.

References

1. World Health Organization (WHO). Online. Available from: http://www.who.int/mediacentre/factsheets/fs297/en/. (Accessed December, 2018).
2. American Cancer Society. Breast cancer facts & figures 2012–2014. *Breast Cancer Facts Fig*. 2013. doi:10.1007/s10549-012-2018-4.Mesothelin
3. Siegel R. Cáncer Statistics. *Ca Cáncer J*. 2017;67(1):7–30. doi:10.3322/caac.21387
4. Pugazhendhi A, Edison TNJI, Karuppusamy I, Kathirvel B. Inorganic nanoparticles: a potential cancer therapy for human welfare. *Int J Pharm*. 2018;539(1–2):104–111. doi:10.1016/j.ijpharm.2018.01.034
5. Ruggiero C, Metter EJ, Cherubini A, et al. White blood cell count and mortality in the baltimore longitudinal study of aging. *J Am Cardio*. 2007;50(18):1810–1850. doi:10.1016/j.jacc.2007.01.076
6. Long M, Tao S, Vega D, et al. Nrf2-dependent suppression of azoxymethane/dextran sulfate sodium–induced colon carcinogenesis by the cinnamon-derived dietary factor cinnamaldehyde. *Cancer Prev Res*. 2015;8(5):444–454. doi:10.1158/1940-6207

7. He XY, Yuan YZ. Advances in pancreatic cancer research: moving towards early detection. *World J Gastroenterol*. 2014;20 (32):11241–11248. doi:10.3748/wjg.v20.i32.11241
8. Vincent A, Herman J, Schulick R, Hruban RH, Goggins M. Pancreatic cancer. *Lancet*. 2011;378(9791):607–620. doi:10.1016/S0140-6736(10)62307-0
9. Masago K, Fukuhara A, Ito Y, et al. Infectious background of febrile advanced lung cancer patients who recieved chemotherapy. *Oncol Lett*. 2010;1(1):109–112. doi:10.3892/ol
10. Cameron AC, Touyz RM, Lang NN. Vascular complications of cancer chemotherapy. *Can J Cardiol*. 2016;32(7):852–862. doi:10.1016/j.cjca.2015.12.023
11. Aahlin EK, Olsen F, Uleberg B, Jacobsen BK, Lassen K. Major postoperative complications are associated with impaired long-term survival after gastro-esophageal and pancreatic cancer surgery: a complete national cohort study. *BMC Surg*. 2016;16(1):1–8. doi:10.1186/s12893-016-0149-y
12. Shanmuganathan R, Edison TNJI, LewisOscar F, Kumar P, Shanmugam S, Pugazhendhi A. Chitosan nanopolymers : an overview of drug delivery against cancer. *Int J Biol Macromol*. 2019;130:727–736. doi:10.1016/j.ijbiomac.2019.02.060
13. Oyebode O, Kandala N, Chilton PJ, Lilford RJ. Use of traditional medicine in middle-income countries : a WHO-SAGE study. *Health Policy Plan*. 2016;31(8):984–991. doi:10.1093/heapol/czw022
14. Payyappallimana U. Role of traditional medicine in primary health care : an overview of role of traditional medicine in primary health care : an overview of perspectives and challenges. *Yokohama Journal of Social Science*. 2010;14(6):57–77.
15. Nasri H, Baradaran A, Shirzad H, Rafieian-Kopaei M. New concepts in nutraceuticals as alternative for pharmaceuticals. *Int J Prev Med*. 2014;5(12):1487–1499. Available from:: http://www.ncbi.nlm.nih.gov/pmc/articles/PMC4336979/.
16. Nune SK, Chanda N, Shukla R, et al. Green nanotechnology from tea: phytochemicals in tea as building blocks for production of biocompatible gold nanoparticles. *J Mater Chem*. 2009;19 (19):2912–2920. doi:10.1039/B822015H
17. Shukla R, Nune SK, Chanda N, et al. Soybeans as a phytochemical reservoir for the production and stabilization of biocompatible gold nanoparticles. *Small*. 2008;4(9):1425–1436. doi:10.1002/smll.200800525
18. Xiang L, Xiao L, Wang Y, Li H, Huang Z, He X. Health benefits of wine: don't expect resveratrol too much. *Food Chem*. 2014;156:258–263. doi:10.1016/j.foodchem.2014.01.006
19. Berman AY, Motechin RA, Wiesenfeld MY, Holz MK. The therapeutic potential of resveratrol: a review of clinical trials. *NPJ Precis Oncol*. 2017;1(1):35. doi:10.1038/s41698-017-0038-6
20. Dong W, Zhou Y, Yang Z. Research progress of mechanism of action of resveratrol. *Pharmacology Pharm*. 2016;7:170–175. doi:10.4236/pp.2016.74022
21. Borriello A. Resveratrol in cancer prevention and treatment: focusing on molecular targets and mechanism of action. *Proceedings*. 2017;1 (10):976. doi:10.3390/proceedings1100976
22. Anisimova NYU, Kiselevsky MV, Sosnov AV, Sadovnikov SV, Stankov IN, Gakh AA. A comparative study. *Chem Cent J*. 2011;5 (1):88. doi:10.1186/1752-153X-5-88
23. Gambini J, Inglés M, Olaso G, Abdelaziz KM, Vina J, Borras C. Properties of resveratrol : in vitro and in vivo studies about metabolism, bioavailability, and biological effects in animal models and humans. *Oxid Med Cell Longev*. 2015. doi:10.1155/2015/837042
24. Allan KE, Lenehan CE, Ellis AV. UV light stability of -cyclodextrin /resveratrol hostguest complexes and isomer stability at varying pH. *Aust J Chem*. 2009;62(8):921–926. doi:10.1071/CH08506
25. Owen A, Moscatelli D, Lovell JF, Katti KV, Mazza M. The application of nanotechnology in medicine: treatment and diagnostics. *Nanomedicine (Lond)*. 2014;9:1291–1294. doi:10.2217/nnm.14.93
26. Shukla R, Chanda N, Zambre A, Upendran A, Katti K, Kulkarni RR. Laminin receptor specific therapeutic gold efficacy in treating prostate cancer. *PNAS*. 2012;1–6. doi:10.1073/pnas.1121174109
27. Mccormack DR, Bhattacharyya K, Kannan R, Katti K. Enhanced photoacoustic detection of melanoma cells using gold nanoparticles. *Lasers Surg Med*. 2011;338(March):333–338. doi:10.1002/lsm.21060
28. Chanda N, Kattumuri V, Shukla R, et al. Bombesin functionalized gold nanoparticles show in vitro and in vivo cancer receptor specificity. *Proc Natl Acad Sci USA*. 2010. doi:10.1073/pnas.1002143107
29. Chanda N, Kan P, Watkinson LD, et al. Radioactive gold nanoparticles in cancer therapy : therapeutic efficacy studies of GA- 198 AuNP nanoconstruct in prostate tumor – bearing mice. *Nanomed Nanotechnol Biol Med*. 2010;6(2):201–209. doi:10.1016/j.nano.2009.11.001
30. Boote E, Fent G, Kattumuri V, et al. Gold nanoparticle contrast in a phantom and juvenile swine: models for molecular imaging of human organs using x-ray computed tomography. *Acad Radiol*. 2010;17(4):410–417. doi:10.1016/j.acra.2010.01.006
31. Chanda N, Shukla R, Katti KV, Kannan R. Gastrin releasing protein receptor specific gold nanorods : breast and prostate tumor avid nanovectors for molecular imaging. *Nano Lett*. 2009;9 (5):1798–1805. doi:10.1021/nl8037147
32. Fent GM, Casteel SW, Kim Y, et al. Biodistribution of maltose and gum arabic hybrid gold nanoparticles after intravenous injection in juvenile swine. *Nanomed Nanotechnol Biol Med*. 2009;5(2):128–135. doi:10.1016/j.nano.2009.01.007
33. Katti KK, Kattumuri V, Bhaskaran S, Katti KV, Kannan R. Facile and general method for synthesis of sugar-coated gold nanoparticles. *Int J Green Nanotechnol Biomed*. 2009;1(1):B53–B59. doi:10.1080/19430850902983848
34. Katti K, Chanda N, Shukla R, et al. Green nanotechnology from cumin phytochemicals: generation of biocompatible gold nanoparticles. *Int J Green Nanotechnol Biomed*. 2009;1(1):B39–B52. doi:10.1080/19430850902931599
35. Kattumuri V, Katti K, Bhaskaran S, et al. Gum arabic as a phytochemical construct for the stabilization of gold nanoparticles: in vivo pharmacokinetics and X-ray-contrast-imaging studies. *Small*. 2007;3(2):333–341. doi:10.1002/smll.200600427
36. Sinha S, McKnight D, Katti KV, et al. Gold nanoparticles stabilized in gum arabic for corneal gene therapy. *Invest Ophthalmol Vis Sci*. 2008;49(13):4787. doi:10.1167/iovs.07-0624
37. Katti KV, Kannan R, Katti K, et al. Hybrid gold nanoparticles in molecular imaging and radiotherapy. *Czech J Phys*. 2006;56(4):D23. doi:10.1007/s10582-006-0484-9
38. Katti KV, Khoobchandani M, Thipe VC, et al. Prostate tumor therapy advances in nuclear medicine : green nanotechnology toward the design of tumor specific radioactive gold nanoparticles. *J Radioanal Nucl Chem*. 2018;318(3):1737–1747. doi:10.1007/s10967-018-6320-4
39. Katti KV, Kannan R, Katti KK, Chanda N, Shukla R, inventor; University of Missouri System, assignee. Soy, lentil or extract stabilized, biocompatible gold nanoparticles. United States Patent US 9694032. 2017 Jul 4.
40. Gamal-Eldeen AM, Moustafa D, El-Daly SM, et al. Gum Arabic-encapsulated gold nanoparticles for a non-invasive photothermal ablation of lung tumor in mice. *Biomed Pharmacother*. 2017;89:1045–1054. doi:10.1016/j.biopha.2017.03.006
41. Geraldes AN, Alves A, Leal J, et al. Green nanotechnology from plant extracts: synthesis and characterization of gold nanoparticles. *Adv Nanopart*. 2016;176–185. doi:10.4236/anp.2016.53019
42. Gamal-Eldeen AM, Moustafa D, El-Daly SM, et al. Photothermal therapy mediated by gum Arabic-conjugated gold nanoparticles suppresses liver preneoplastic lesions in mice. *J Photochem Photobiol B Biol*. 2016;163:47–56. doi:10.1016/j.jphotobiol.2016.08.009
43. You A, Be MAY, In I. Agarose-stabilized gold nanoparticles for surface-enhanced Raman spectroscopic detection of DNA nucleosides. 2015:153114. doi:10.1063/1.2192573

44. Khoobchandani M, Zambre A, Katti K, Lin C, Katti KV. Green nanotechnology from brassicaceae : development of broccoli phytochemicals – encapsulated gold nanoparticles and their applications in nanomedicine. *Int J Green Nano*. 2013. doi:10.1177/1943089213509474
45. Suganthy N, Sri Ramkumar V, Pugazhendhi A, Benelli G, Archunan G. Biogenic synthesis of gold nanoparticles from Terminalia arjuna bark extract: assessment of safety aspects and neuroprotective potential via antioxidant, anticholinesterase, and anti-amyloidogenic effects. *Environ Sci Pollut Res*. 2018;25 (11):10418–10433. doi:10.1007/s11356-017-9789-4
46. Price NPJ, Vermillion KE, Eller FJ, Vaughn SF. Frost Grape Polysaccharide (FGP), an emulsion-forming arabinogalactan gum from the stems of native north american grape species vitis riparia michx. *J Agric Food Chem*. 2015. doi:10.1021/acs.jafc.5b02316
47. Granzotto C, Arslanoglu J, Rolando C, Tokarski C. Plant gum identification in historic artworks. *Nat Publ Gr*. 2017;1–15. doi:10.1038/srep44538
48. Cornelsen PA, Quintanilha RC, Vidotti M, Gorin PAJ, Simas-Tosin FF, Riegel-Vidotti IC. Native and structurally modified gum arabic: exploring the effect of the gum's microstructure in obtaining electroactive nanoparticles. *Carbohydr Polym*. 2015;119:35–43. doi:10.1016/j.carbpol.2014.11.020
49. Betzer O, Perets N, Angel A, et al. In Vivo neuroimaging of exosomes using gold nanoparticles. *ACS Nano*. 2017;11 (11):10883–10893. doi:10.1021/acsnano.7b04495
50. Zhang Q, Iwakuma N, Sharma P, et al. Gold nanoparticles as a contrast agent for *in vivo* tumor imaging with photoacoustic tomography. *Nanotechnology*. 2009;20(39):395102. doi:10.1088/0957-4484/20/39/395102
51. Zhang Y, Chu W, Foroushani AD, et al. New gold nanostructures for sensor applications: A review. *Materials (Basel)*. 2014;7 (7):5169–5201. doi:10.3390/ma7075169
52. Selim ME, Hendi A. Gold nanoparticles induce apoptosis in MCF-7 human breast cancer cells. *Asian Pac J Cancer Prev*. 2012;13 (4):1617–1620. doi:10.7314/APJCP.2012.13.4.1617
53. Ali MRK, Wu Y, Tang Y, et al. Targeting cancer cell integrins using gold nanorods in photothermal therapy inhibits migration through affecting cytoskeletal proteins. *Proc Natl Acad Sci*. 2017;114(28): E5655–E5663. doi:10.1073/pnas.1703151114
54. Spadavecchia J, Movia D, Moore C, et al. Targeted polyethylene glycol gold nanoparticles for the treatment of pancreatic cancer: from synthesis to proof-of-concept in vitro studies. *Int J Nanomedicine*. 2016;11:791–822. doi:10.2147/IJN.S97476
55. Khoo AM, Cho SH, Reynoso FJ, et al. Radiosensitization of prostate cancers in vitro and in vivo to erbium-filtered orthovoltage x-rays using actively targeted gold nanoparticles. *Sci Rep*. 2017;7(1):18044. doi:10.1038/s41598-017-18304-y
56. Calavia PG, Chambrier I, Cook MJ, Haines AH, Field RA, Russell DA. Targeted photodynamic therapy of breast cancer cells using lactose-phthalocyanine functionalized gold nanoparticles. *J Colloid Interface Sci*. 2018;512(SupplementC):249–259. doi:10.1016/j.jcis.2017.10.030
57. Au M, Emeto T, Power J, Vangaveti V, Lai H. Emerging therapeutic potential of nanoparticles in pancreatic cancer: a systematic review of clinical trials. *Biomedicines*. 2016;4(3):20. doi:10.3390/biomedicines4030020
58. Tamarkin LI, Kingston DG. Exposing the tumor microenvironment: how gold nanoparticles enhance and refine drug delivery. *Ther Deliv*. 2017;8(6):363–366. doi:10.4155/tde-2016-0095
59. Kodiha M, Mahboubi H, Maysinger D, Stochaj U. Gold nanoparticles impinge on nucleoli and the stress response in MCF7 breast cancer cells. *Nanobiomedicine*. 2016;3:3. doi:10.5772/62337
60. Lee J, Chatterjee DK, Leeb MH, Krishnana S. Gold nanoparticles in breast cancer treatment: promise and potential pitfalls. *Cancer Lett*. 2014;347(1):46–53. doi:10.1016/j.canlet.2014.02.006.Gold
61. Ko J, Sethi G, Um J, et al. The role of resveratrol in cancer therapy. *Int J Mol Sci*. 2017;(1–36). doi:10.3390/ijms18122589
62. Varoni EM, Lo Faro AF, Sharifi-Rad J, Iriti M. Anticancer molecular mechanisms of resveratrol. *Front Nutr*. 2016;3:8. doi:10.3389/fnut.2016.00008
63. Iqbal J, Abbasi BA, Mahmood T, Kanwal S, Ali B, Shah SA. Asian Paci fi c Journal of Tropical Biomedicine. *Asian Pac J Trop Biomed*. 2017;7(12):1129–1150. doi:10.1016/j.apjtb.2017.10.016
64. Xiao Q, Zhu W, Feng W, Lee SS, Leung AW. A review of resveratrol as a potent chemoprotective and synergistic agent in cancer chemotherapy. *Front Pharmacol*. 2019;9:1–10. doi:10.3389/fphar.2018.01534
65. Imran M, Butt MS, Nadeem M, Peters DG, Mubarak MS. Resveratrol as an anti-cancer agent: A review AU - Rauf, Abdur. *Crit Rev Food Sci Nutr*. 2018;58(9):1428–1447. doi:10.1080/10408398.2016.1263597
66. Murakami Y, Kawata A, Ito S, Katayama T, Fujisawa S. The radical scavenging activity and cytotoxicity of resveratrol, orcinol and 4-allylphenol and their inhibitory effects on cox-2 gene expression and Nf-κb Activation in RAW264.7 Cells stimulated with porphyromonas gingivalis -fimbriae. *In Vivo*. 2015;350:341–349.
67. Pasanphan W, Rattanawongwiboon T, Choofong S, Güven O, Katti KK. Irradiated chitosan nanoparticle as a water-based antioxidant and reducing agent for a green synthesis of gold nanoplatforms. *Radiat Phys Chem*. 2015;106:360–370. doi:10.1016/j.radphyschem.2014.08.023
68. Baronzio G, Parmar G, Baronzio M. Overview of methods for overcoming hindrance to drug delivery to tumors, with special attention to tumor interstitial fluid. *Front Oncol*. 2015;5:1–17. doi:10.3389/fonc.2015.00165
69. Jain RK, Stylianopoulos T. Delivering nanomedicine to solid tumors. *Nat Publ Gr*. 2010;7(11):653–664. doi:10.1038/nrclinonc.2010.139
70. Mittapalli RK, Adkins CE, Mohammad A, Lockman PR, Virginia W. Quantitative fluorescence microscopy measures vascular pore size in primary and metastatic brain tumors. *Cancer Res*. 2018;77 (2):238–246. doi:10.1158/0008-5472.CAN-16-1711